Master of Science Thesis

Path Integral Monte Carlo Simulation of Helium-4 Nanodroplets

Marcus Ahlström

Supervisor: Mats Wallin

Department of Theoretical Physics,
School of Engineering Sciences
Royal Institute of Technology, SE-106 91 Stockholm, Sweden

Stockholm, Sweden 2015

Typeset in LaTeX

Examensarbete inom ämnet teoretisk fysik för avläggande av civilingenjörsexamen inom utbildningsprogrammet Teknisk fysik.

Graduation thesis on the subject Theoretical Physics for the degree of Master of Science in Engineering from the School of Engineering Sciences.

TRITA-FYS 2015:43
ISSN 0280-316X
ISRN KTH/FYS/–15:43–SE

Printed in Sweden by Universitetsservice US AB, Stockholm June 2015

Abstract

Quantum effects in many-body systems of ^{4}He at low temperature are studied in a two dimensional droplet geometry using a path integral simulation of worldlines of ^{4}He atoms. The implementation of an effective Metropolis-Hastings algorithm is discussed in some detail.

We investigate the dependency on multiple parameters: droplet diameter, worldline lengths, number of particles involved, and investigate their effects on the energy, heat capacity and RMS-distance between particles. The cases of Bose-Einstein and Boltzmann statistics, and of interacting and free systems are compared.

We find that Bose-Einstein statistics start affecting the interacting systems around 3K, a much higher temperature than expected. We discuss the implication the finite-size space and low density of the simulation volumes may have on these results. The free systems have small differences in energy, with a larger difference in heat capacity than expected, likely due to finite-size effects. The RMS-distance shows that the lack of periodic boundary allows the particles to escape their respective potential wells, and diffuse to the domain walls.

We also discuss possible future extensions to three dimensions, calculation of superfluid density, and effects of entanglement on the entropy.

Keywords: Path Integral Monte Carlo, Metropolis algorithm, helium-4, Bose-Einstein statistics, superfluidity.

Preface

This thesis is the result of my Master's degree project at the Department of Theoretical Physics during the spring and early fall 2014. The work concerns Path Integral Monte Carlo (PIMC) simulations of ^{4}He in the temperatures just above 1 Kelvin on a two dimensional droplet geometry.

This thesis is divided into six chapters and one appendix. Chapter 1 briefly discusses the historical discovery of superfluidity in helium, which is the main application for PIMC simulations. Chapter 2 outlines Feynman's path integral formulation of quantum mechanics and the theoretical framework for statistical sampling. Chapter 3 derives the expression of the system action, and explains the isomorphism with a polymer chain. Chapter 4 outlines the sampling method of the Monte Carlo algorithm. In Chapter 5, we present the results of the simulations. Finally, in Chapter 6, we summarize the results.

In Appendix A, we analytically solve the quantum mechanical particle in a box problem on a circular domain.

In this thesis, we will use the natural unit conventions , with $\hbar = 1$ and $k_B = 1$, thus measuring energy in Kelvin. Particles obeying Maxwell-Boltzmann statistics will be called *boltzmannons*, similarly to how particles obeying Bose-Einstein statistics being commonly referred to as *bosons*.

Acknowledgements

First and foremost, I would like to thank my advisor Prof. Mats Wallin for giving me the opportunity to work on this project, for his valuable feedback and guidance, and for always taking time when I come asking questions, no matter how trivial they were. Furthermore, his constant support and understanding for my personal health has been nothing short of invaluable.

I want to thank Dr. Hannes Meier for his help and guidance in the start of the project, and for introducing me to the subject of Path Integral Monte Carlo simulations. I also want to thank Dr. Jack Lidmar for all technical support he has offered throughout my project.

I would also like to thank all the Ph.D. and Master students at the Department of Theoretical Physics for helping me feel included in the group, making it that much more fun to come to the office. Special thanks to Jessica Elevant for the valuable and fun discussions, no matter if they were about teaching, quantum field theory, or Doctor Who.

Finally I would like to thank my parents Sverker and Elisabeth, my grandparents Gerd and Bengt, and my sisters Axelia and Emelie, for their support throughout my university years and life.

Contents

To Robyn, my wife-to-be.
Your love brightens even the darkest days

Chapter 1

Introduction

Superfluid helium was discovered independently by P. Kapitsa [1], and by J.F. Allen and D. Misener [2] in 1938, when helium was cooled down in the liquid phase. Classically an element is expected to make a transition from a liquid to a solid state at sufficiently a sufficiently low temperature for a given pressure. However, in the case of helium kept below a pressure of 25 bar the transition from liquid to solid state never seem to happen. Instead, the liquid starts to show new properties below 2.17K only expected in a Bose-Einstein condensate. The viscosity becomes zero, and its heat capacity becomes infinite. When the fluid is put in a rotating container in this state, it creates quantized vortices. These characteristics have dubbed this state as a new phase of matter called the *superfluid* state.

In an experimental setting, there are only two elements that so far have produced a superfluid state, ^{4}He and ^{3}He. Theoretically, hydrogen should also become superfluid at low temperatures, but the element is too reactive for this to have been confirmed in experiments.

When the viscosity of the helium cooled below the $\lambda-$line (see Fig. 1) is measured, it is in fact, not zero. This is explained in modern theory by the *two-fluid model*, where a fraction of the helium becomes superfluid, and the other stays in a normal liquid state. If the superfluid and liquid states are separated, a fraction of the superfluid will transition to a normal liquid state to reach the equilibrium fraction of superfluid helium.

In most good heat conductors, such as copper, the high heat conduction is attributed to the presence of a valence band. In superfluid ^{4}He, no such band exists. In the superfluid, heat flow is instead determined by a wave equation similar to how sound propagates in air.

Superfluid ^{4}He also exhibits a creeping effect, where if the liquid is kept in an

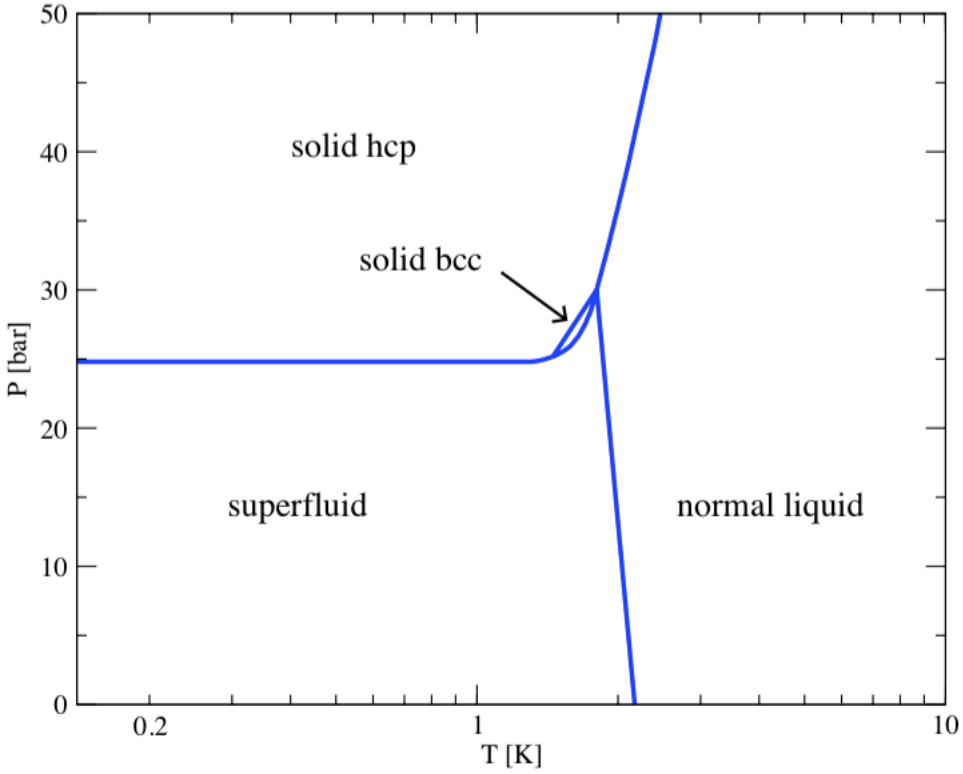

Figure 1.1. Phase diagram for ^{4}He. The boundary line between the liquid and superfluid states is called the *λ-line*, which peaks at $T = 2.172$K, the so called *λ-point*.

open container it will creep up the walls, working against the gravitational force, and escape. This requires careful construction of special containers for the superfluid. Once it escapes confinement, it immediately evaporates without boiling upon reaching the warmer regions, due to the high heat capacity.

These examples show that strong quantum effects in helium lead to new and interesting macroscopic properties, much like superconducting states of matter do. Quantum effects such as these at temperatures below 1K are very difficult and time consuming to accurately capture in computer simulations. Often times, these effects are not accounted for in the temperature ranges above 1K (see for example Ref. [3]). In this thesis we investigate systematically what is the magnitude of the error involved in neglecting these quantum effects. We will demonstrate that these effects have a non-neglible effect on the energy, heat capacity and RMS-distance between particles at temperatures below 3K.

Chapter 2

Background

In this chapter we will introduce path integral formulation of quantum mechanics, as well as the basics of statistical sampling of a physical system. In this chapter we forgo the convention used in the rest of the thesis, and instead use standard SI-units.

2.1 Path integral formulation of quantum mechanics

In 1948 Feynman described quantum mechanics using path integrals [4]. Quantum mechanics had previously been formulated in independent, equivalent formulations by Heisenberg's matrix mechanics in 1925 [5] and Schrödinger's wave mechanics in 1926 [6]. Feynman's formulation generalized the classical action of a system defined as

$$\mathcal{S}[x(t)] = \int_0^t \mathrm{d}t' \mathcal{L}, \tag{2.1}$$

where $\mathcal{L} = \mathcal{L}[x_0(t'), \dot{x}_0(t'), \ddot{x}_0(t'), ...x_{n-1}(t'), \dot{x}_{n-1}(t')..., t']$ is the Lagrangian of the system. In a classical system, a single path which extremizes the action determines the system dynamics. But in quantum mechanics, this is not true. The realization of Feynman was that in quantum mechanics all possible paths contribute to the action of the system. He formulated that the probability

$$P(x_0, x_1; t_1 - t_0) = \left|U(x_0, x_1; t)\right|^2, \tag{2.2}$$

of a particle to propagate from a point (t_0, x_0) to (t_1, x_1) is given by

$$U(x_0, x_1; t) = \sum_{\text{all paths}} \frac{1}{N} \exp\left\{\frac{i}{\hbar} S\left[x\left(t\right)\right]\right\}, \tag{2.3}$$

where N is a normalizing constant, $t = t_1 - t_0$. We can convert the sum to a Riemann integral by discretizing the action in M time slices of width $\tau = |x_i - x_{i-1}|$. In the limit $\tau \to 0$ we get

$$U(x_0, x_1; t) = \lim_{\tau \to 0} \frac{1}{N} \int \cdots \int \frac{\mathrm{d}x_1}{N} \cdots \frac{\mathrm{d}x_{M-1}}{N} \exp\left(\frac{i}{\hbar} S\left[x(t)\right]\right), \tag{2.4}$$

or more compactly

$$U(x_0, x_1; t) = \int_0^1 \mathcal{D}x(t) \exp\left(\frac{i}{\hbar} S\left[x(t)\right]\right), \tag{2.5}$$

where $\mathcal{D}x(t) = \frac{1}{N^M} \mathrm{d}x_1 \cdots \mathrm{d}x_{M-1}$.

The functional $U(x_0, x_1; t)$ is a propagator that determines the time evolution of the particle. The wave function for the particle at position x_1 and time t_1 can thus be expressed as

$$\psi(x_1, t_1) = \int_{-\infty}^{\infty} \mathrm{d}x_0 U(x_0, x_1; t) \psi(x_0, t_0). \tag{2.6}$$

If we define t_1 as an incremental increase τ from t_0, and using the expression for the classical Lagrangian $\mathcal{L} = m\dot{x}^2/2 - V(x, t)$, we can express Eq.(2.6) as

$$\psi(x_1, t_0 + \tau) = \int_{-\infty}^{\infty} \mathrm{d}x_0 \exp\left(\frac{i}{\hbar} \frac{m(x_1 - x_0)^2}{\tau}\right) \exp\left(-\frac{i\tau}{\hbar} V(x_0, t)\right) \psi(x_0, t_0), \tag{2.7}$$

under the assumption that

$$\int_0^{\tau} \mathrm{d}t V(x, t) = \tau V(x, t). \tag{2.8}$$

With the substitution $x_0 = x_1 + \chi$, we can expand the above expression in a power series in τ. The series to first order become

$$\psi(x_1, t_0 + \tau) + \tau \frac{\partial}{\partial t} \psi(x_1, t_0 + \tau) = \frac{1}{N} \int_{-\infty}^{\infty} \mathrm{d}\chi \exp\left(\frac{im\chi^2}{\hbar\tau}\right) \left(1 - \frac{i\tau}{\hbar} V(x_0, t)\right)$$
$$\times \left(\psi(x_1, t_0 + \tau) + \chi \frac{\partial}{\partial x_1} \psi(x_1, t_0 + \tau) + \chi^2 \frac{\partial^2}{\partial {x_1}^2} \psi(x_1, t_0 + \tau)\right). \tag{2.9}$$

In order to be correct to zeroth order, we require that

$$\frac{1}{N} \int_{-\infty}^{\infty} \mathrm{d}\chi \exp\left(\frac{im\chi^2}{\hbar\tau}\right) = 1 \tag{2.10}$$

$$N = \sqrt{\frac{2\pi i \hbar \tau}{m}} \tag{2.11}$$

At first order we then get

$$\psi(x,t) + \tau\frac{\partial\psi}{\partial t}(x,t) = \psi(x,t) - \frac{i\tau}{\hbar}V(x,t)\psi(x,t) + \frac{\hbar\tau}{2im}\frac{\partial^2\psi}{\partial x^2}(x,t), \tag{2.12}$$

which means the $\psi(x,t)$ must satisfy

$$i\hbar\frac{\partial\psi}{\partial t} = -\frac{\hbar^2}{2m}\frac{\partial^2\psi}{\partial x^2} + V\psi, \tag{2.13}$$

which is just the Schrödinger equation. We have thus shown the equivalence between the path integral formulation of quantum mechanics, with the familiar wave formulation by Schrödinger.

2.1.1 The density matrix

Moving away from the single-particle formalism for a system with N particles, we exchange x_i for $R_i = \{\mathbf{r}_{i,0}\dots\mathbf{r}_{i,N-1}\}$. The position-space density matrix for a many-body system is given as

$$\rho(R_0,R_1;\beta) = \langle R_1|\, e^{-\beta H}\,|R_0\rangle = \sum_i \phi_i^*(R_0)\phi_i(R_1)e^{-\beta E_i}. \tag{2.14}$$

The product of two density matrices is a density matrix [7]

$$\langle R_2|\left(e^{-\beta_0 H}e^{-\beta_1 H}\right)|R_0\rangle = \langle R_2|\, e^{-(\beta_0+\beta_1)H}\,|R_0\rangle\,, \tag{2.15}$$

or equivalently

$$\rho(R_0,R_2;\beta_0+\beta_1) = \int \mathrm{d}R_1\rho(R_0,R_1;\beta_0)\rho(R_1,R_2;\beta_1). \tag{2.16}$$

Using this we can discretize the the path integral in M time slices

$$e^{-\beta H} = \left(e^{-\tau H}\right)^M, \tag{2.17}$$

where we have defined the *imaginary time step* $\tau = \beta/M$. In position space the exact density matrix becomes a convolution of $M-2$ integrals

$$\rho(R_0,R_M;\beta) = \int\cdots\int \mathrm{d}R_1\cdots R_{M-1}\rho(R_0,R_1;\tau)\cdots\rho(R_{M-1},R_M;\tau). \tag{2.18}$$

2.1.2 Connection between density matrix and time evolution

In the last step we talked about the discretizaion of inverse temperature $\beta = k_B T$ as *imaginary time*. This is due to the relationship between the density matrix and

the time evolution propagator. Taking the derivative of Eq (2.14) with respect to β

$$\frac{\partial}{\partial\beta}\rho(R_0, R_1; \beta) = \sum_i -E_i\phi_i^*(R_0)\phi_i(R_1)e^{-\beta E_i}, \tag{2.19}$$

we end up with the Bloch equation

$$\frac{\partial}{\partial\beta}\rho(R_0, R_1; \beta) = \left(-\frac{\hbar^2}{2m}\frac{\partial^2}{\partial {R_0}^2} + V(R_0)\right)\rho(R_0, R_1; \beta) \tag{2.20}$$

This is very similar to the Schrödinger equation. In fact, since the propagator must obey the Schrödinger equation

$$i\hbar\frac{\partial}{\partial t}U(x_0, x_1; t) = \left(-\frac{\hbar^2}{2m}\frac{\partial^2}{\partial x^2} + V\right)U(x_0, x_1; t) \tag{2.21}$$

we arrive at the *equivalence*

$$\rho(R_0, R_1; \beta) = U(x_0, x_1; -i\beta\hbar). \tag{2.22}$$

To summarize, what we have done is transform the Minkowski space to an Euclidian space by first performing a Wick-rotation

$$t \to -it \tag{2.23}$$

and then inserting the substitution

$$\beta = \frac{1}{k_B T} = t/\hbar, \tag{2.24}$$

which explains the earlier reference to τ as an imaginary time step.

2.2 Sampling

Many-body systems have a high number of possible states allowed by the laws of physics. The naive way of calculating physical properties would be by calculating every single configuration's contribution. This is not feasible to do in any non-trivial systems. All configurations do not contribute equally though. In fact, the success of statistical mechanics is that a few configurations are so much more overwhelmingly probable than others that we can deduce the physical properties from the dominating configurations alone. This makes it very suitable to use a Monte Carlo method. In order to get reliable data without needing to spend too much time to calculate, we need to be able to pick out these configurations that contribute most. The act of choosing these configurations is called *importance sampling*.

2.2.1 Stationary processes and detailed balance

The physical system is said to reach equilibrium when it becomes *stationary*, i.e., when the Master equation

$$\frac{\mathrm{d}\pi}{\mathrm{d}t} = \sum_s \pi(s,t)P(s \to s') - \pi(s',t)P(s' \to s), \tag{2.25}$$

is equal to zero. Here $\pi(s,t)$ denotes the probability of the system to be in state s at time t, and $P(s \to s')$ the probability for the system to transition from the state s to s'. To satisfy Eq. (2.25) being zero, it is sufficient that we attain *detailed balance*, i.e.,

$$\pi(s)P(s \to s') = \pi(s')P(s' \to s), \tag{2.26}$$

where the time dependency has been omitted.

In the computer simulation, the starting configuration is pre-determined, but the end results should be independent of this choice. We must therefore let the algorithm warm up and run for a while before data is collected. By making sure the algorithm satisfies detailed balance, we can be sure that the system eventually reaches this equilibrium. Once we are certain that the algorithm satisfies detailed balance, the remaining problem is to optimize it to reach the equilibrium as fast as possible.

2.2.2 Metropolis-Hastings algorithm

A Monte Carlo simulation is a general term for any type of algorithm that uses repeated random samplings. In this thesis, we will make use of the so called *Metropolis-Hastings algorithm* [8], or just "Metropolis-algorithm" for short. The Metropolis algorithm follows detailed balance, where Eq. (2.26) can be rewritten as

$$\frac{P(s \to s')}{P(s' \to s)} = \frac{\pi(s')}{\pi(s)}. \tag{2.27}$$

We can factorize the transition probability as

$$P(s \to s') = T(s \to s')A(s \to s'), \tag{2.28}$$

where $T(s \to s')$ is an *a priori* known transition probability from s to s', and $A\,(s \to s')$ is the probability of accepting such a transition. Equation (2.27) thus takes the form

$$\frac{A(s \to s')}{A(s' \to s)} = \frac{T(s' \to s)\pi(s')}{T(s \to s')\pi(s)}. \tag{2.29}$$

We see that we do not need to know the individual acceptance probabilities, but only the ratio $\frac{A(s \to s')}{A(s' \to s)}$. We can therefore set one of the acceptance probabilities to

1, say $A(s' \to s) = 1$, and still obey detailed balance. The acceptance test for the algorithm becomes

$$A(s \to s') = \min \left[1, \ \frac{T(s' \to s)\pi(s')}{T(s \to s')\pi(s)}\right]. \tag{2.30}$$

The Metropolis algorithm can be summarized as follows [9]

1. Pick a state s at random
2. Generate a state s' according to $T(s \to s')$
3. Generate a random number $0 \leq r < 1$
4. If $A(s \to s') \geq r$, the state transitions $s \to s'$
5. If $A(s \to s') < r$, the state is left unchanged, and nothing is updated.

For a system of N particles, we need to perform N iterations of the algorithm above before every time-step update. We call it a time-step update when we collect data on the system, energy, heat capacity etc. Thus, for every iteration, we allow for the possibility of every particle in the system to update at least once.

Remark: Due to the limitations of deterministic computers, with the term *random* number, we in practice mean a *pseudo-random*. In the implementation, we use a Mersenne Twister algorithm to generate a uniform distribution of pseudo-random numbers between 0 and 1 (see Ref. [10]).

Chapter 3

Action

The PIMC algorithm can be summarized as having three parts: action, sampling and properties to measure. We will outline each part in the following chapters. In this chapter, we will construct the action of the system. We will end the chapter by discussing the isomorphism between the quantum mechanical particles and classical polymers.

3.1 Discrete density matrix

First, we need to construct the action for the system. We can make an approximation of the exact density matrix in Eq (2.18) by using the Trotter forumla [11]

$$e^{-\beta H} = e^{-\beta(T+V)} = \lim_{M\to\infty} \left[e^{-\tau T} e^{-\tau V}\right]^M , \tag{3.1}$$

which is true if T, V and $T+V$ are self-adjoint and bounded from below [7], which is true for all systems are that obey Boltzmann or Bose-Einstein statistics. In the limit of large M, the density matrix from Eq. (2.18) becomes

$$\rho(R_0, R_M; \tau) = \int \mathrm{d}R_1 \ldots \mathrm{d}R_{M-1} \prod_{j=0}^{M-1} \sum_i \langle R_j | \, e^{-\tau T} \, | R_i \rangle \, \langle R_i | \, e^{-\tau V} \, | R_{j+1} \rangle \, , \tag{3.2}$$

We remember that $R_i = \{\mathbf{r}_{i,0} \ldots \mathbf{r}_{i,N-1}\}$. We can evaluate the matrices in this representation. The potential operator is diagonal [7]

$$\langle R_i | \, e^{-\tau V} \, | R_j \rangle = e^{-\tau V(R_i)} \delta(R_j - R_i), \tag{3.3}$$

whereas the kinetic operator is obtained from solving the eigenvalue problem

$$T \, |k_i\rangle = \lambda k_i^2 \, |k_i\rangle \, . \tag{3.4}$$

where $\lambda = \hbar^2/2m = 6.0596 \text{Å}^2$ K for ^{4}He. Using $\langle R_i | k_n \rangle = L^{-dN/2} e^{i k_n \cdot R_i}$ and $k_n = \left(\frac{2\pi n}{L}\right)$, where d is the number of spatial dimensions, and n is a $d \cdot N-$dimensional

integer vector, the eigenvalue problem can be solved by transforming to momentum space

$$\begin{aligned}\langle R_i|\, e^{-\tau T}\, |R_j\rangle =& \sum_{n=0}^{\infty} \langle R_i|\, e^{-\tau T}\, |k_n\rangle \langle k_n|R_j\rangle \\ =& \sum_{n=0}^{\infty} \exp\left(-\tau\left(\lambda k_n^2\right)\right) \langle R_i|k_n\rangle \langle k_n|R_j\rangle \\ =& L^{-dN} \sum_{n=0}^{\infty} \exp\left(-\tau\lambda k_n^2 - ik_n\left((R_j - R_i)\right)\right). \end{aligned} \tag{3.5}$$

We approximate the sum as an integral for $L \longrightarrow \infty$, $L^{-1} = \mathrm{d}k/2\pi$

$$\begin{aligned}\langle R_i|\, e^{-\tau T}\, |R_j\rangle =& \int \frac{\mathrm{d}^{dN}k}{(2\pi)^{dN}} \exp\left(-\tau\lambda k_n^2 - ik_n(R_j - R_i)\right) \\ =& \int \frac{\mathrm{d}^{dN}k}{(2\pi)^{dN}} \exp\left(-\tau\lambda\left(k_n - \frac{i\left(R_j - R_i\right)}{2\tau\lambda}\right)^2 - \frac{\left(R_j - R_i\right)^2}{4\tau\lambda}\right) \\ =& \left(4\pi\tau\lambda\right)^{dN/2} \exp\left(-\frac{\left(R_j - R_i\right)^2}{4\tau\lambda}\right). \end{aligned} \tag{3.6}$$

Using these results, we can get a discrete expression for the density matrix in position space

$$\rho(R_0, R_M; \beta) = \int \mathrm{d}R_1 \cdots \mathrm{d}R_{M-1} \left(4\pi\tau\lambda\right)^{dNM/2} \exp\left[-\sum_{i=0}^{M}\left(\frac{\left(R_{i+1} - R_i\right)^2}{4\lambda\tau} + \tau V(R_i)\right)\right]. \tag{3.7}$$

3.1.1 The polymer isomorphism

From the definition of the equivalence in Eq. (2.22), we define the action S_μ of the μ :th link in the chain as

$$\begin{aligned} S_\mu =& -\log\left(\rho\left(R_{\mu+1}, R_\mu; \tau\right)\right) \\ =& \frac{dN}{2}\log\left(4\pi\tau\lambda\right) + \frac{\left(R_{\mu+1} - R_\mu\right)^2}{4\lambda\tau} + \tau V(R_\mu). \end{aligned} \tag{3.8}$$

The action is separated into three terms. The first term is exactly the action predicted by the classical equipartition theorem. The second is a kinetic "spring-term", and the third is a potential term. This is similar to the modelling of polymers [12], by means of separating the kinetic "spring" action from the potential. We can

thus imagine the quantum particle as a polymer chain, where the total action is given as a sum of all links

$$S = \frac{dNM}{2} \log\left(4\pi\tau\lambda\right) + \sum_{n=0}^{M} \frac{\left(R_{n+1} - R_n\right)^2}{4\lambda\tau} + \tau \sum_{n=0}^{M} V(R_n) \tag{3.9}$$

The above approximation of the action is a direct consequence of Trotter's formula (3.1). As such, it is only exact in the limit $M \longrightarrow \infty$. The problem with long chains is that the runtime increases, since the Metropolis algorithm will do $N \cdot M$ iteration between every time step update, since every bead is now a "particle" that interacts with all other particles in the same time step, as well as the previous and next particle on the bead-polymer. The challenge will be to create a way to sample the algorithm to get reliable data in i quick manner, while keeping the number of beads as short as possible.

3.1.2 Approximating the interaction term

Some explanation is warranted for the approximation(s) of the interaction of particles. We will use the *primitive approximation*, that each particle pair's interaction is independent of the other particles.

We model the interaction between two ^{4}He with the *Aziz potential* [13], given by

$$V\left(r\right) = \epsilon\left(a \cdot e^{-\alpha x} - h\left[\frac{c_6}{x^6} + \frac{c_8}{x^8} + \frac{c_{10}}{x^{10}}\right]\right) \tag{3.10}$$

$$h = \begin{cases} 1 & \text{if } x > d \\ e^{-\left(\frac{d}{x} - 1\right)^2} & \text{if } x < d \end{cases} \tag{3.11}$$

where the parameters are$x = \frac{|r|}{2.9673\ \text{Å}}$, $\epsilon = 10.8$ K, $a = 0.54485046 \cdot 10^6$, $\alpha = 13.353384$, $c_6 = 1.3732412$, $c_8 = 0.4253785$, $c_{10} = 0.1781$, $d = 1.241314$. The Aziz potential is plotted in Fig. 3.1. In order to make the algorithm run faster, we make a linear approximation of the potential

$$V(R) = \frac{V(R_i) - V(R_{i+1})}{2}, \tag{3.12}$$

where $R_i \leq R < R_{i+1}$. Higher order corrections can be done to the action to fasten the convergence rate further (see Ref. [3,7]), but is not implemented in the work of this thesis.

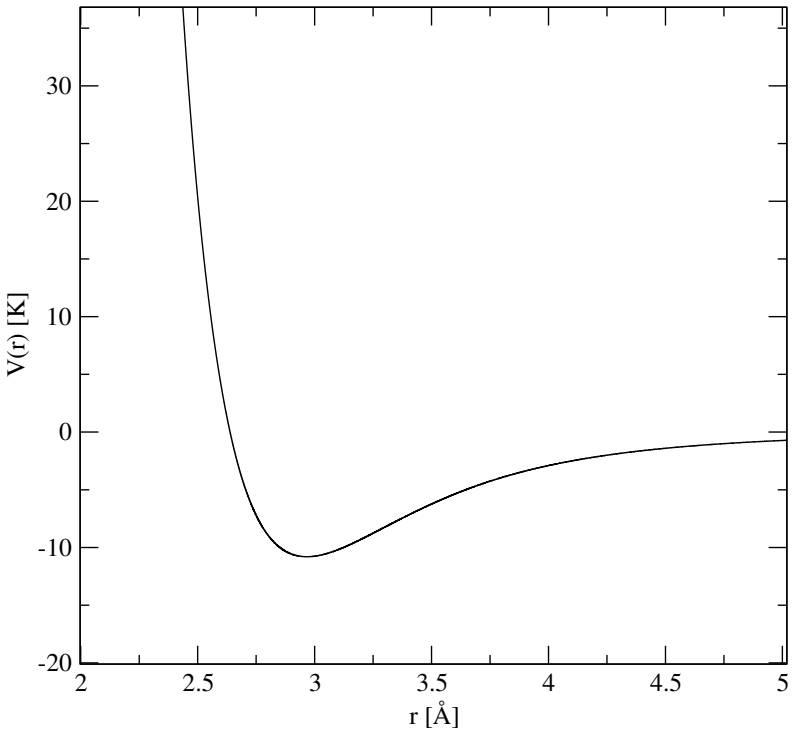

Figure 3.1. Aziz potential for the pair wise interaction between ^{4}He atoms. The potential is expressed in natural units, $\hbar = k_B = 1$.

Chapter 4

Sampling

In this chapter, we will begin with investigating how to sample the system of distinguishable particles. The sampling techniques will be further developed in the the last section of this chapter to treat indistinguishable particles. The system of particles can perform two different moves in every time step. Individual beads can be moved on the particle worldlines, or a whole world line can be translated in space. For a given system of N particles with M beads each, we need to perform $N \cdot M$ iterations of the bead movement, and N iterations of the the world line translation, for every time step of the algorithm [9].

4.1 Bead movements

In this section we discuss Monte Carlo moves for beads on the particle world line. We start with the simple moves for individual beads, and then the improved bisection method and multi-level Metropolis algorithm [14]. Another sampling method not used worth mentioning is the method of staging (see Ref. [15]).

4.1.1 Bead-by-bead sampling

The simplest form of sampling is the method where we update only a single bead at a time. The algorithm starts with randomly choosing a particle k and a bead ν. Setting the *a priori* transition probability $T(s' \to s) = T(s \to s')$ (however, other choices of T are just as viable) and set the probabilities to

$$\pi(s) = \frac{\exp\left(-\sum_{\mu=1}^{M} S_\mu\right)}{Z}, \tag{4.1}$$

where $Z = \int \mathrm{d}R\rho(R, R; \beta)$ is the partition function. Since the partition functions is defined as a trace over ρ, we need to add a periodic boundary condition $R_0 = R_M$

for Eq. (3.7).

For reasons that will be clear, we choose the displacement to be normally distributed around the mean $\bar{\mathbf{r}}_k = \frac{1}{2}\left(\mathbf{r}_{\nu-1,k} + \mathbf{r}_{\nu+1,k}\right)$ with variance σ^2

$$T(s \to s') = \frac{1}{\sqrt{2\pi\sigma^2}} \exp\left(-\frac{\left(\mathbf{r}'_{\nu k} - \bar{\mathbf{r}}_k\right)^2}{2\sigma^2}\right), \tag{4.2}$$

$$T(s' \to s) = \frac{1}{\sqrt{2\pi\sigma^2}} \exp\left(-\frac{\left(\mathbf{r}_{\nu k} - \bar{\mathbf{r}}_k\right)^2}{2\sigma^2}\right). \tag{4.3}$$

After the bead has been displaced, The action of the new position is compared with the acceptance criterion

$$A(s \to s') = \min\left[1, \frac{T(s' \to s)\exp\left(-\sum_{\mu=1}^{M} S'_\mu\right)}{T(s \to s')\exp\left(-\sum_{\mu=1}^{M} S_\mu\right)}\right]. \tag{4.4}$$

Since the only term in the sum to proposed to change is $S_\nu \to S'_\nu$, the acceptance simplifies to

$$\begin{aligned}
&\frac{T(s' \to s)\exp\left(-\sum_{\mu=1}^{M} S'_\mu\right)}{T(s \to s')\exp\left(-\sum_{\mu=1}^{M} S_\mu\right)} \\
&= \exp\left(-\frac{\left(\mathbf{r}'_{\nu k} - \bar{\mathbf{r}}_k\right)^2}{2\sigma^2} + \frac{\left(\mathbf{r}_{\nu k} - \bar{\mathbf{r}}_k\right)^2}{2\sigma^2}\right) \\
&\quad \times \exp\left(\frac{\sum_{\mu=\nu}^{\nu+1}\left(\mathbf{r}_{\mu k} - \mathbf{r}_{\mu-1 k}\right)^2 - \sum_{\mu=\nu}^{\nu+1}\left(\mathbf{r}'_{\mu k} - \mathbf{r}'_{\mu-1 k}\right)^2}{4\lambda\tau}\right) \\
&\quad \times \exp\left(-\tau\left[V\left(\mathbf{r}'_{\nu k}\right) - V\left(\mathbf{r}_{\nu k}\right)\right]\right).
\end{aligned} \tag{4.5}$$

The middle exponential can be simplified as

$$\begin{aligned}
&\exp\left(\frac{\sum_{\mu=\nu}^{\nu+1}\left(\mathbf{r}_{\mu k} - \mathbf{r}_{\mu-1 k}\right)^2 - \sum_{\mu=\nu}^{\nu+1}\left(\mathbf{r}'_{\mu k} - \mathbf{r}'_{\mu-1 k}\right)^2}{4\lambda\tau}\right) \\
&= \exp\left(\frac{1}{2\lambda\tau}\left[\mathbf{r}'^2_{\nu k} - 2\mathbf{r}'_{\nu k}\bar{\mathbf{r}}_k - \mathbf{r}^2_{\nu k} + 2\mathbf{r}_{\nu k}\bar{\mathbf{r}}_k\right]\right) \\
&= \exp\left(\frac{1}{2\lambda\tau}\left[\left(\mathbf{r}'_{\nu k} - \bar{\mathbf{r}}_k\right)^2 - \left(\mathbf{r}_{\nu k} - \bar{\mathbf{r}}_k\right)^2\right]\right).
\end{aligned} \tag{4.6}$$

Setting the variance of $T(s \to s')$ to $\sigma^2 = \lambda\tau$ gives the simple expression for the acceptance probability

$$A(s \to s') = \min\left[1, e^{-\tau\left(V\left(\mathbf{r}'_{\nu k}\right) - V\left(\mathbf{r}_{\nu k}\right)\right)}\right]. \tag{4.7}$$

If a move is accepted, all thermodynamic averages of interest are incrementally

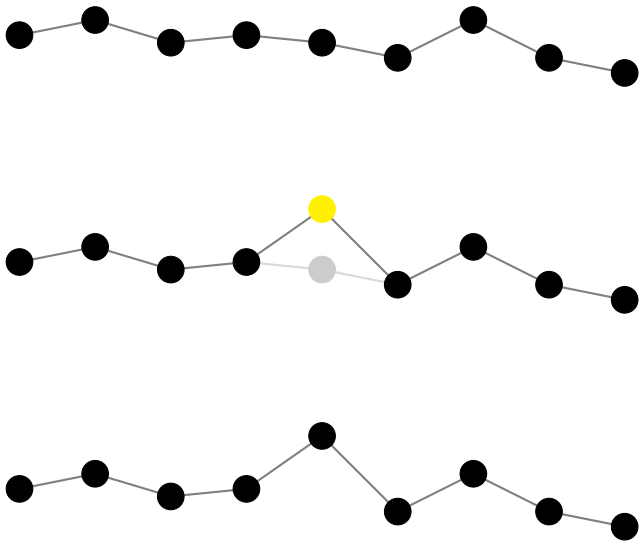

Figure 4.1. Bead-by-bead movement of the worldline. The middle bead is moved if the proposed move is accepted

adjusted. If it is rejected, nothing more is done. Even if the move is rejected, the configuration of the system contributes to the thermal averages of the system.

The method of moving individual beads one by one has a number of drawbacks. An accepted move only changes the system slightly, and if the same bead were to be chosen to be moved again, it has a very high probability of moving back to the same position, since any move such that $-\Delta S_\nu = S'_\nu - S_\nu > 0$ is always accepted. This can lead to to increasing CPU run-times before the system reaches equilibrium, and at lower temperatures the CPU run-time will scale as M^3 [7].

4.1.2 Multi-level Metropolis algorithm

To improve the sampling, we use a bisection method to implement a multi-level Metropolis algorithm. The idea is that instead of moving a single bead on a world line, we simultaneously move a whole segment of particles. We do not want to make big movements that increases the total action too much, as it is very unlikely to pass the acceptance criterion, and we would spend too much computer resources on attempts that do not update the system. The way we work around this is to perform Metropolis tests successively through the algorithm. If the algorithm fails a single one of the tests, the whole move is rejected, no matter of when it occurs in the algorithm.

We determine a set length of the segment that we want to move. We require

that the number of beads in a move is $2^l + 1$, where l is called the number of *levels* of the algorithm. In the following outline we have used $l = 3$, however this can be fine tuned to fit the system one simulates. A small number of levels will lead to higher acceptance rate for the algorithm. The tradeoff is that small moves distort the chain very little, especially if the chain contains hundreds or thousands of beads. A good goal is to have as many levels as possible while keeping the acceptance between $20 - 50\%$ [16].

Using the proposed $l = 3$ we pick a particle k and bead ν at random. This bead will be the first of the segment. We fix this particle, and the last particle of the segment. We then ignore all beads in between them, except for the bead in the middle. This bead is moved as if the time step was four times larger than usual

$$\mathbf{r'}_{\nu+4,k} = \frac{1}{2}\left(\mathbf{r}_{\nu,k} + \mathbf{r}_{\nu+8,k}\right) + \eta\sqrt{4\lambda\tau}, \tag{4.8}$$

where $\eta\sqrt{4\lambda\tau} \sim \mathcal{N}(0, 4\lambda\tau)$. The extra factor 4 in the variance is due to the time step being 4 times larger than usual. After the new position has been generated, we check the acceptance criterion

$$A_{l=3}(s \to s') = \min\left[1, e^{-4\tau\left(V(\mathbf{r'}_{\nu+4,k}) - V(\mathbf{r}_{\nu+4,k})\right)}\right]. \tag{4.9}$$

If this trail move fails the acceptance test, the algorithm does not attempt any more moves. If it succeeds, we have a new position for the $\nu + 4$ bead. We now set the level to $l = 2$ and redo the same process. The fixed beads now are the ν:th, $\nu+4$:th and $\nu + 8$:th beads

$$\mathbf{r'}_{\nu+2,k} = \frac{1}{2}\left(\mathbf{r}_{\nu,k} + \mathbf{r'}_{\nu+4,k}\right) + \eta\sqrt{2\lambda\tau} \tag{4.10}$$

$$\mathbf{r'}_{\nu+6,k} = \frac{1}{2}\left(\mathbf{r'}_{\nu+4,k} + \mathbf{r}_{\nu+8,k}\right) + \eta\sqrt{2\lambda\tau}. \tag{4.11}$$

When we check the acceptance criterion for this level, we must take into account that we have already accepted the movement of the $\nu+4$:th particle in the previous step

$$\begin{aligned} &A_{l=2}(s \to s') \\ =&\min\left[1, e^{-2\tau\sum_{j=1}^{3}\left(V(\mathbf{r'}_{\nu+2j,k}) - V(\mathbf{r}_{\nu+2j,k})\right)} e^{4\tau\left(V(\mathbf{r'}_{\nu+4,k}) - V(\mathbf{r}_{\nu+4,k})\right)}\right]. \end{aligned} \tag{4.12}$$

Again, if the trial moves fail the test at this level, it leaves the system in its initial state.

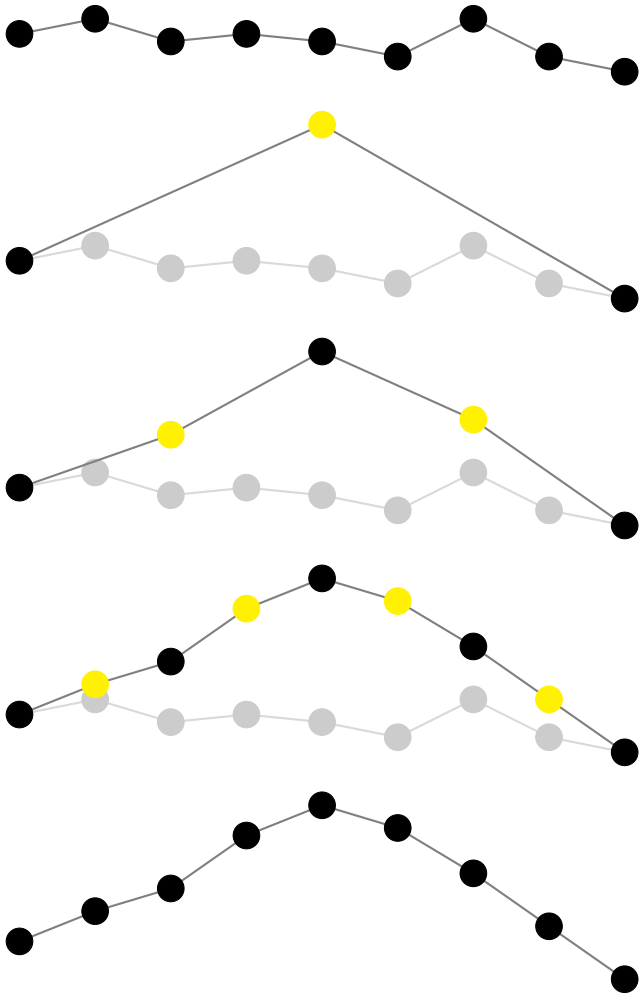

Figure 4.2. The multi-level Metropolis algorithm with three levels. If the full move is accepted, the total distortion of the chain is much greater than gained with the single bead move.

At the final level, $l = 1$, we move all 4 beads that have been left so far

$$\mathbf{r'}_{\nu+1,k} = \frac{1}{2}\left(\mathbf{r}_{\nu,k} + \mathbf{r'}_{\nu+2,k}\right) + \eta\sqrt{\lambda\tau} \tag{4.13}$$

$$\mathbf{r'}_{\nu+3,k} = \frac{1}{2}\left(\mathbf{r'}_{\nu+2,k} + \mathbf{r}_{\nu+4,k}\right) + \eta\sqrt{\lambda\tau} \tag{4.14}$$

$$\mathbf{r'}_{\nu+5,k} = \frac{1}{2}\left(\mathbf{r}_{\nu+4,k} + \mathbf{r'}_{\nu+6,k}\right) + \eta\sqrt{\lambda\tau} \tag{4.15}$$

$$\mathbf{r'}_{\nu+7,k} = \frac{1}{2}\left(\mathbf{r'}_{\nu+6,k} + \mathbf{r}_{\nu+8,k}\right) + \eta\sqrt{\lambda\tau}. \tag{4.16}$$

and the acceptance test

$$\begin{aligned} &A_{l=1}(s \to s') \\ &= \min\left[1, e^{-\tau\sum_{i=1}^{7}\left(V(\mathbf{r'}_{\nu+i,k}) - V(\mathbf{r}_{\nu+i,k})\right)} e^{2\tau\sum_{j=1}^{3}\left(V(\mathbf{r'}_{\nu+2j,k}) - V(\mathbf{r}_{\nu+2j,k})\right)}\right]. \end{aligned} \tag{4.17}$$

The total acceptance rate becomes

$$\begin{aligned} A(s \to s') =& A_{l=3}(s \to s')A_{l=2}(s \to s')A_{l=1}(s \to s') \\ =& e^{-4\tau\left(V(\mathbf{r'}_{\nu+4,k}) - V(\mathbf{r}_{\nu+4,k})\right)} \\ & \times e^{-2\tau\sum_{j=1}^{3}\left(V(\mathbf{r'}_{\nu+2j,k}) - V(\mathbf{r}_{\nu+2j,k})\right)} e^{4\tau\left(V(\mathbf{r'}_{\nu+4,k}) - V(\mathbf{r}_{\nu+4,k})\right)} \\ & \times e^{-\tau\sum_{i=1}^{7}\left(V(\mathbf{r'}_{\nu+i,k}) - V(\mathbf{r}_{\nu+i,k})\right)} e^{2\tau\sum_{j=1}^{3}\left(V(\mathbf{r'}_{\nu+2j,k}) - V(\mathbf{r}_{\nu+2j,k})\right)} \\ =& e^{-\tau\sum_{i=1}^{7}\left(V(\mathbf{r'}_{\nu+i,k}) - V(\mathbf{r}_{\nu+i,k})\right)}, \end{aligned} \tag{4.18}$$

which is the same result as moving the beads one by one in Eq. (4.7), thus obeying detailed balance.

We could just as well have let the algorithm accept all cases until the final level, and then test against the exact acceptance criterion, while still obeying detailed balance. However, this would lose the efficiency gain of discarding bad configurations early in the simulation.

4.1.3 Worldline movement

The worldline can also be displaced as a whole by moving its center of mass. We now only look at the center of mass of the particles $\mathbf{r}_k = \frac{1}{M}\sum_{\nu=0}^{M-1} m r_{\nu k}$. Moving any of these particles only costs potential energy.

$$\begin{aligned} A(s \to s') &= \min\left[1, e^{-\tau M\left(V(\mathbf{r'}_k) - V(\mathbf{r}_k)\right)}\right] \\ &= \min\left[1, e^{-\beta\mathcal{H}_{cm}}\right], \end{aligned} \tag{4.19}$$

which is what we expect from a classical particle. In high temperature limit $\beta \to 0$, these classical movements' contributions to the action will be dominating. In the

domain we are interested in $\beta > 1/10$, this contribution will be small. In the case of indistinguishable particles (bosons and fermions), the implementation of this part is made much harder. The small contribution of this move in the regions of interest for this thesis motivates us to skip it in the case for bosons and fermions.

4.2 Worldline swaps

In this section we outline the unique quantum mechanical property of bosons and fermions: indistinguishability. In the path integral interpretation, this is manifested by particle worldlines to attaching themselves to each other, and together form a new worldline that runs to laps around the time-axis. Thus, two or more particle worldlines can connect and form a combined worldline that circles itself two "laps" around the imaginary time axis.

To achieve this, the algorithm will cyclically exchange $1 < n \leq N$ particle worldlines. Worldline k will be connected with k' between beads ν and $\nu + s$, where s is optimally chosen as the same number as used in the multi-level Metropolis algorithm [16]. The algorithm is divided in two parts. First we move through permutation space, choosing which particles will be included in the cycle. In the second parts, we connect worldlines with each other. Both parts have multiple acceptance tests, which must all be passed for the algorithm to continue.

The technique described in Ref. [14] is commonly used in the literature to implement worldline permutations. However, we adopt the method described in Ref. [16] since it is easier to implement.

4.2.1 Constructing the permutation cycle

The permutation cycle is constructed by first randomly choosing a particle k, and bead ν to start with. The bead ν could be anywhere on the worldline, if it happens to be near the end, the bead $\nu + s$ is subjected to the periodic boundary condition in imaginary time. This can lead to problems if one is not careful, since the bead $\nu + s$ might be on another worldline k'' that k has been entangled with earlier.

After the particle and bead have been selected, we set up a table over the free-particle density matrices for the particle to entangle with other worldlines m

$$\begin{aligned} K_{km}^{(1)} =& \rho_F\left(\mathbf{r}_{k\nu}, \mathbf{r}_{m,\nu+s}; s\tau\right)\left(1-\delta_{km}\right) \\ =& \exp\left(-s\frac{\left(\mathbf{r}_{m,\nu+s}-\mathbf{r}_{k\nu}\right)^2}{4\lambda\tau}\right)\left(1-\delta_{km}\right), \end{aligned} \tag{4.20}$$

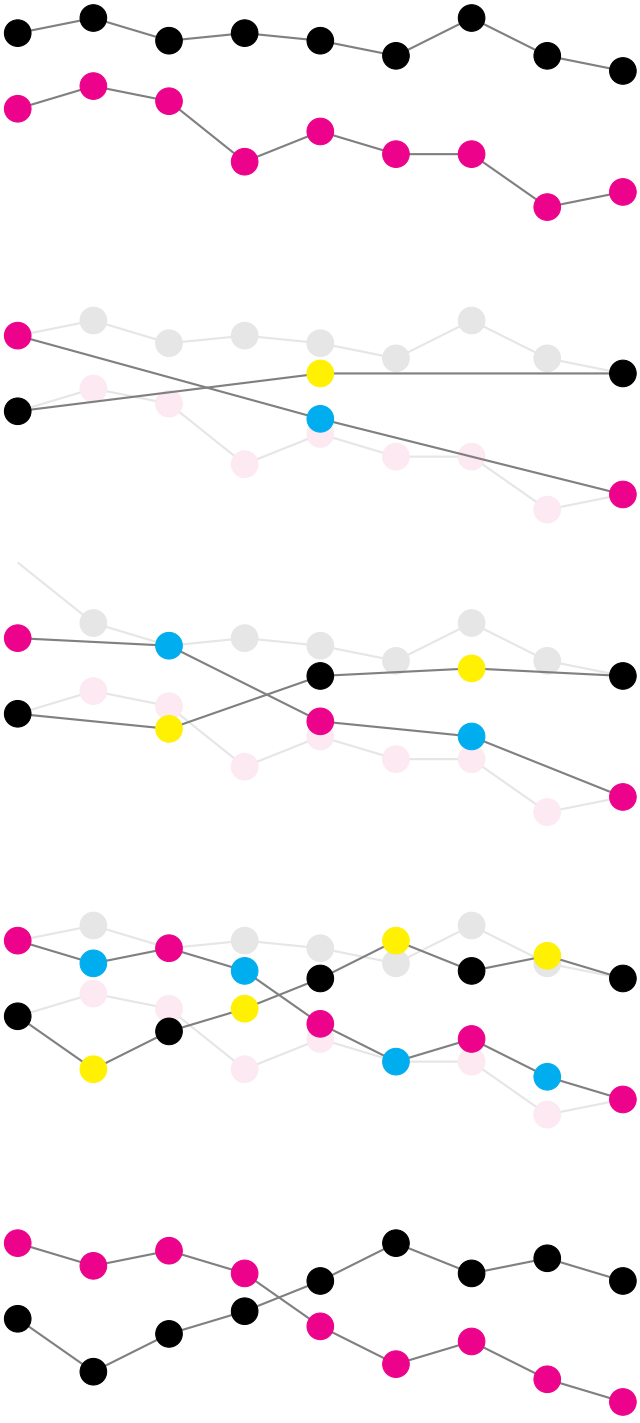

Figure 4.3. The world line swap between two worldlines. The worldline paths between the endpoints of the segments are constructed using the multi-level Metropolis algorithm.

note that the density matrix of the identity permutation is not included. The acceptance criterion becomes

$$A^{(1)} = \frac{\sum_m K^{(1)}_{km}}{\sum_m K^{(1)}_{km} + \rho\left(\mathbf{r}_{k\nu}, \mathbf{r}_{k,\nu+s}; s\tau\right)}. \tag{4.21}$$

If the trial move fails this acceptance criterion, the process is aborted, if it passes, then a particle q will be chosen as the particle that k exchanges to with probability

$$\Pi_q = \frac{K^{(1)}_{kq}}{\sum_m K^{(1)}_{km}}. \tag{4.22}$$

In the next step, we create a new table $K^{(2)}_{qm}$

$$K^{(2)}_{qm} = \rho_F\left(\mathbf{r}_{q\nu}, \mathbf{r}_{m,\nu+s}; s\tau\right)\left(1 - \delta_{qm}\right), \tag{4.23}$$

and the corresponding acceptance criterion

$$A^{(2)} = \frac{\sum_m K^{(2)}_{qm}}{\sum_m K^{(2)}_{qm} + \rho\left(\mathbf{r}_{q\nu}, \mathbf{r}_{q,\nu+s}; s\tau\right)}. \tag{4.24}$$

If the algorithm fails at this point, the whole process is aborted. If it passes, a new particle for the cycle p is chosen with probability

$$\Pi_p = \frac{K^{(2)}_{qp}}{\sum_m K^{(2)}_{qm}}. \tag{4.25}$$

This now has a chance to give us $p = k$. If this happens, the permutation cycle is complete, and we move on to construct the paths between the worldlines of the particles. If $p \neq k$, we move on creating another table

$$K^{(3)}_{pm} = \rho_F\left(\mathbf{r}_{p\nu}, \mathbf{r}_{m,\nu+s}; s\tau\right)\left(1 - \delta_{qm}\right)\left(1 - \delta_{pm}\right). \tag{4.26}$$

with acceptance criterion

$$A^{(3)} = \frac{\sum_m K^{(3)}_{pm}}{\sum_m K^{(3)}_{qm} + \rho\left(\mathbf{r}_{p\nu}, \mathbf{r}_{p,\nu+s}; s\tau\right) + \rho\left(\mathbf{r}_{q\nu}, \mathbf{r}_{q,\nu+s}; s\tau\right)} \tag{4.27}$$

Now we see we do not accept a permutation to *any* other particle already included in the cycle. This process is repeated until it completes the cycle with particle k, or until the algorithm fails an acceptance test.

4.2.2 Constructing particle paths

To construct a the particle path between $\mathbf{r}_{k\nu}$ and $\mathbf{r}_{q,\nu+s}$, we use the multi-level Metropolis algorithm from Sec. 4.1.2. As previously mentioned, care must be taken if $k + s > M$, so that the algorithm samples the correct worldline when it passes the periodic boundary of the time axis, as it may already be entangled from earlier. In every step, the action from all new paths must be taken into account. The acceptance rate for the permutations are very low (see Fig. 5.10), and we generally run tens of thousand attempts in every time-step update.

Chapter 5

Results

In this chapter we present the simulation results. First derivations of the formulas used in the simulation for calculating thermodynamic quantities are considered. We then present results for a test case with two non-interacting particles, and compare it to the predicted analytical results. Finally, we present data for the interacting particles with varying particle numbers.

5.1 Calculating thermodynamic properties

The two thermodynamic properties we are primarily concerned with measuring are the energy and the specific heat capacity. In the Monte Carlo simulation, we need to let the system run until it reaches equilibrium, and then run it a bit further and collect data for the averages. It is quite tedious to find the exact time for when the simulation reaches equilibrium, rather one just overestimates the number of time steps to say 100 000. We then collect data for 6 times as many time steps, making the whole simulation to loop 700 000 times in one run.

5.1.1 Derivation of averages

We derive the energy E of the system from the definition as the expected value of the Hamiltonian

$$\begin{aligned}
E = \langle H \rangle &= -\frac{\partial \log Z}{\partial \beta} = -\frac{1}{Z}\frac{\partial \mathrm{Tr}(e^{-S})}{\partial \beta} \\
&= \frac{1}{Z}\mathrm{Tr}\left(\frac{\partial S}{\partial \beta}e^{-S}\right) = \left\langle \frac{\partial S}{\partial \beta} \right\rangle \\
&= \left\langle \frac{\partial}{\partial \beta}\left(\frac{dNM}{2}\log\left(4\pi\tau\lambda\right) + \sum_{i=0}^{M}\frac{\left(R_{i+1}-R_i\right)^2}{4\lambda\tau} + \tau\sum_{i=0}^{M}V(R_i)\right)\right\rangle \\
&= \left\langle \frac{\partial}{\partial \beta}\left(\frac{dNM}{2}\log\left(4\pi\beta\lambda/M\right) + \sum_{i=0}^{M}\frac{\left(R_{i+1}-R_i\right)^2}{4\lambda\beta/M} + \frac{\beta}{M}\sum_{i=1}^{M}V(R_i)\right)\right\rangle \\
&= \left\langle \frac{dNM}{2\beta} - \frac{M}{4\lambda\beta^2}\sum_{i=0}^{M}\left(R_{i+1}-R_i\right)^2 + \frac{1}{M}\sum_{i=1}^{M}V(R_i)\right\rangle, \qquad (5.1)
\end{aligned}$$

where we used the expression of the action from Eq. (3.8). From this we can get the heat capacity

$$\begin{aligned}
C_V =& \frac{\partial E}{\partial T} = \beta^2\frac{\partial^2 \log Z}{\partial \beta^2} = \beta^2\frac{\partial}{\partial \beta}\left(\frac{1}{Z}\mathrm{Tr}\left(-\frac{\partial S}{\partial \beta}e^{-S}\right)\right) \\
=& \beta^2\left[\frac{1}{Z}\mathrm{Tr}\left(\left[\left(\frac{\partial S}{\partial \beta}\right)^2 - \frac{\partial^2 S}{\partial \beta^2}\right]e^{-S}\right) - \left(\frac{1}{Z}\mathrm{Tr}\left(\frac{\partial S}{\partial \beta}e^{-S}\right)\right)^2\right] \\
=& \beta^2\left(\left\langle E^2\right\rangle - \left\langle \frac{\partial^2 S}{\partial \beta^2}\right\rangle - \langle E\rangle^2\right) \\
=& \beta^2\left(\left\langle E^2\right\rangle - \left\langle -\frac{dNM}{2\beta^2} + \frac{M}{2\lambda\beta^3}\sum_{i=0}^{M}\left(R_{i+1}-R_i\right)^2\right\rangle - \langle E\rangle^2\right). \qquad (5.2)
\end{aligned}$$

The error bars in the plots are for a general thermodynamic average $\langle O \rangle$ at a temperature T given by

$$\frac{\sum_n \langle O^2(T)\rangle_n - \sum_n \langle O(T)\rangle_n^2}{n(T)}, \qquad (5.3)$$

where $\langle O(T)\rangle_1 \ldots \langle O(T)\rangle_n$ are the n measured averages at temperature T, and $n(T)$ are the number of datapoints at temperature T.

5.2 Free particles

We start of with a test case, two non-interacting particles in on a circular disc with hard walls $V(x, y) = 0$, if $\sqrt{x^2 + y^2} < r$, and $V(x, y) = \infty$ everywhere else. The

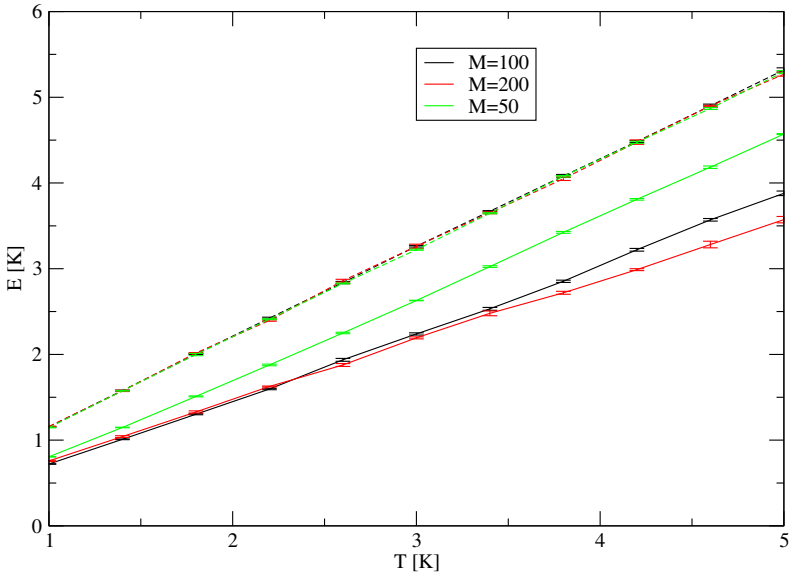

Figure 5.1. The energy levels for two non-interacting particles in the two dimensional disc with 30Å diameter, for varying number of beads on the worldlines.The dotted lines represent boltzmannons, and the solid lines bosons.

problem is analytically solvable (see Appendix A). For boltzmannons and bosons, the ground state can be occupied by multiple particles, and we expect the same energy and heat capacity for both particle types. The solution for the energy and heat capacity depends on the size of the box, and we expect the error in the simulation to depend on the number of time-steps in the path integrals. In Fig. 5.1 through 5.9 we depict boltzmannon data with dotted lines and bosons with solid lines. As we can see in Fig. 5.1, the boltzmannons converge to the same result for all world line lengths, and follow the expected result $E = T$ with only a constant error. From the trend shown in Fig. 5.4, this error seems to grow smaller when the diameter of the simulation volume becomes larger. For the bosons, the constant error seems to be the same at low temperatures for all values of M, but the temperature behavior changes. The bosons may be converging at a faster rate to the other limit, $E = T/2$ (Eq.(A.18)).

The data for the heat capacity has a larger error, due to the dependence on the variance of the energy, the distortion, and length of the worldlines (Eq. (5.2)). For the average RMS-distance between the particles, the boltzmannons do not depend on the size of the simulation volume, but on length of the beads, while the opposite behavior is observed for the bosons.

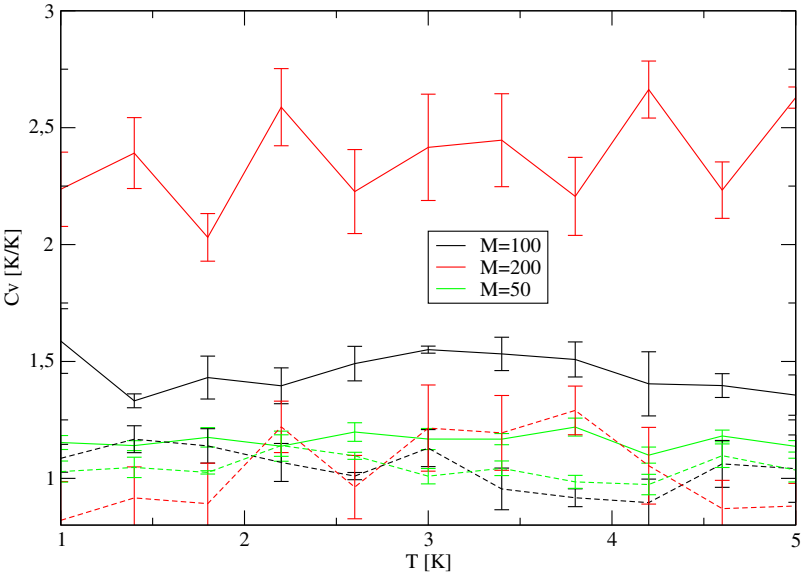

Figure 5.2. The heat capacity for two non-interacting particles in the two dimensional disc with 30Å diameter, for varying number of beads on the worldlines.The dotted lines represent boltzmannons, and the solid lines bosons.

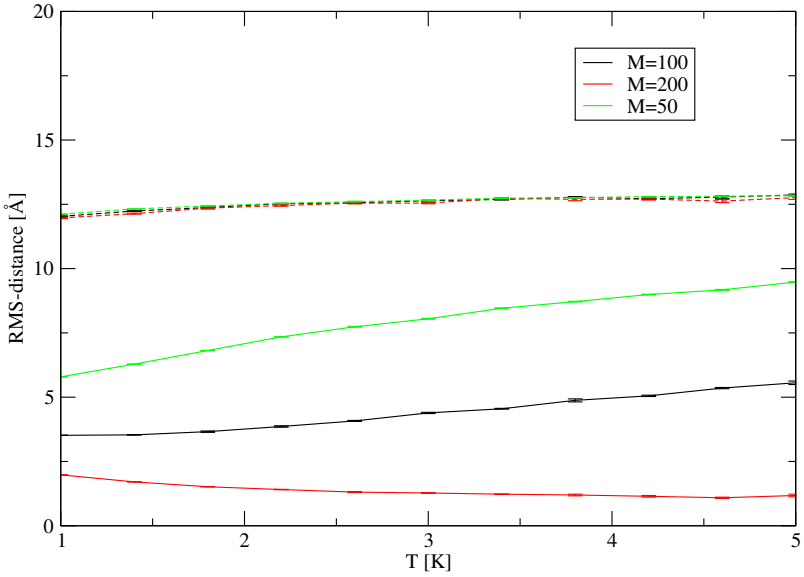

Figure 5.3. The average RMS-distance between two non-interacting particles in the two dimensional disc with 30Å diameter, for varying number of beads on the worldlines.The dotted lines represent boltzmannons, and the solid lines bosons.

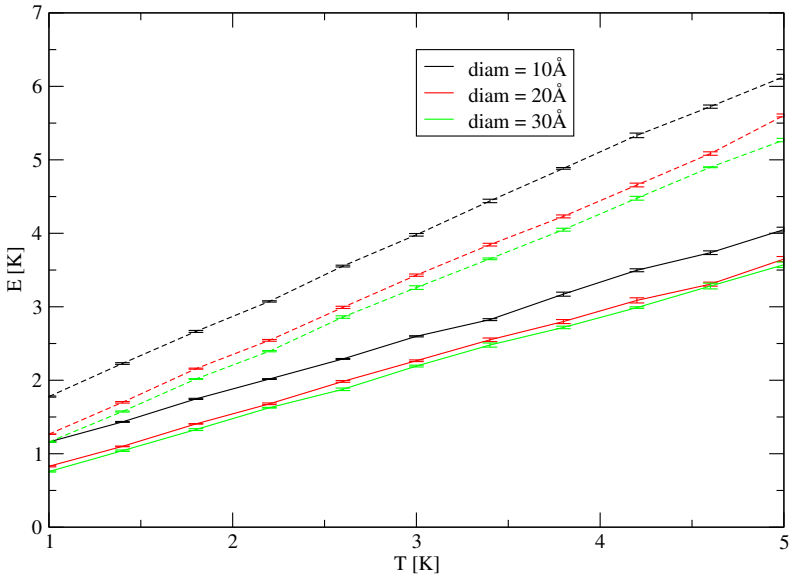

Figure 5.4. The energy levels for two non-interacting particles in the two dimensional disc with varying diameter, for worldlines with 200 beads. The dotted lines represent boltzmannons, and the solid lines bosons.

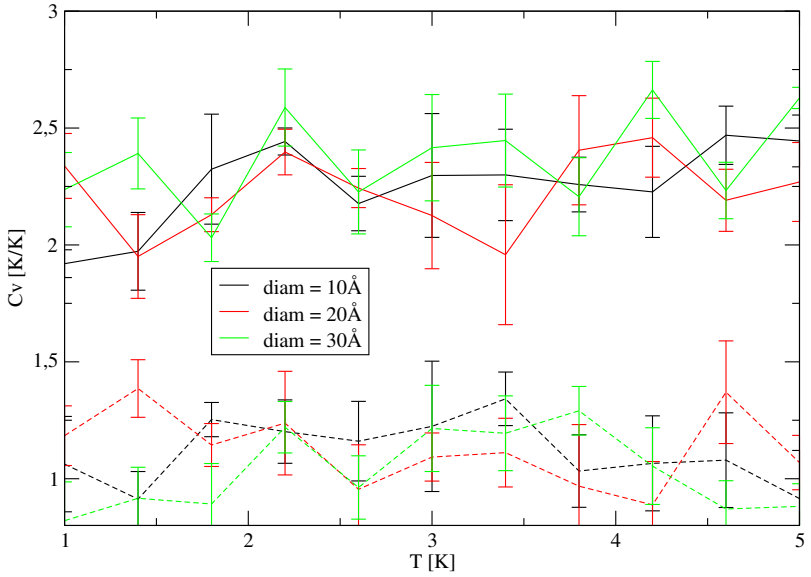

Figure 5.5. The heat capacity for two non-interacting particles in the two dimensional disc with varying diameter, for worldlines with 200 beads. The dotted lines represent boltzmannons, and the solid lines bosons.

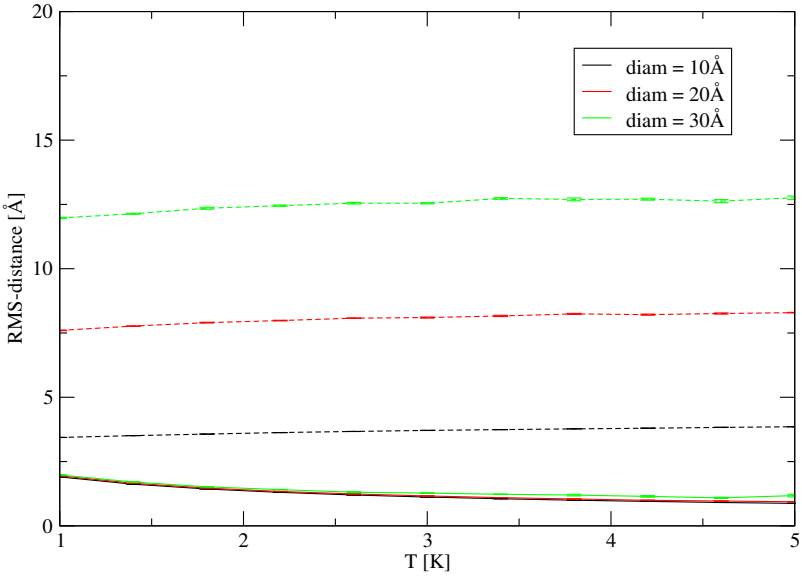

Figure 5.6. The average RMS-distance between two non-interacting particles in the two dimensional disc with varying diameter, for worldlines with 200 beads. The dotted lines represent boltzmannons, and the solid lines bosons.

5.3 Interacting particles

For the next part, we will investigate the central problem, the difference between boltzmannon and boson models for interacting particles. For this part, we will model the interaction with the Aziz potential (Eq. (3.11)). We stress again that we work with the primitive approximation, i.e., that we assume that interaction between two particles is not affected by the other particles in the system.

The energy levels are as expected asymptotically the same in the higher temperature region, but a gap in the energies are apparent below 3K (Fig 5.7), where the heat capacity for the bosons increases whereas it stays near constant for boltzmannons (Fig. 5.8). Geometrically, we notice that the average RMS-distance between the particles is much smaller below 3K for bosons, (Fig 5.9), attributed to the non-zero acceptance rate of the swap move (Fig. 5.10).

There is a clear break of trend between $N = 4$ and $N = 8$ on the small space. It is important to note that the simulations are dealing with a small and confined space, leading to possible finite-size errors. Another explanation could be an ordering of the system resulting in a phase transition when the density becomes high enough.

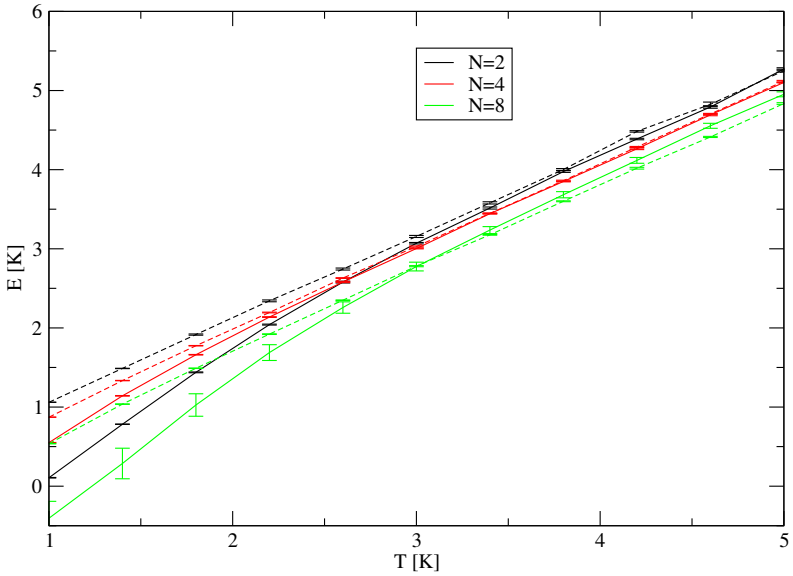

Figure 5.7. The energy levels for different number of interacting particles on a circular volume with diameter 30Å, and with 100 beads on the worldlines.

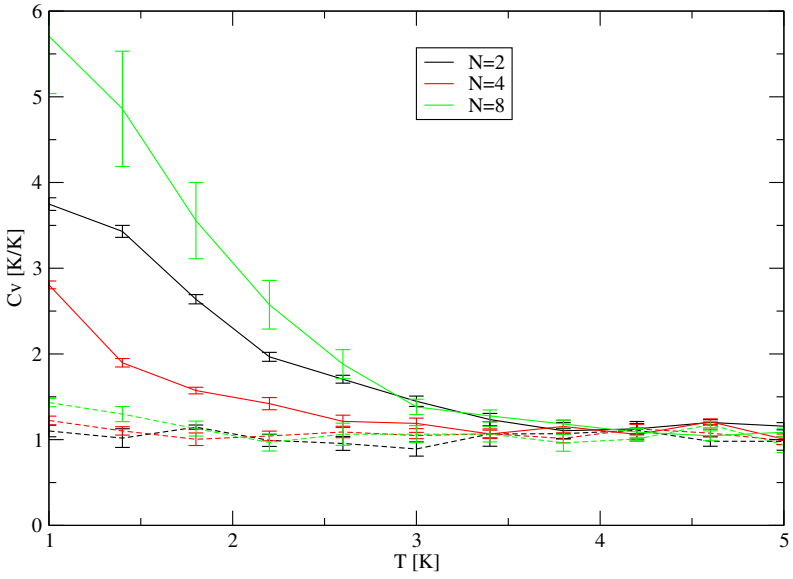

Figure 5.8. The heat capacity for different number of interacting particles on a circular volume with diameter 30Å, and with 100 beads on the worldlines.

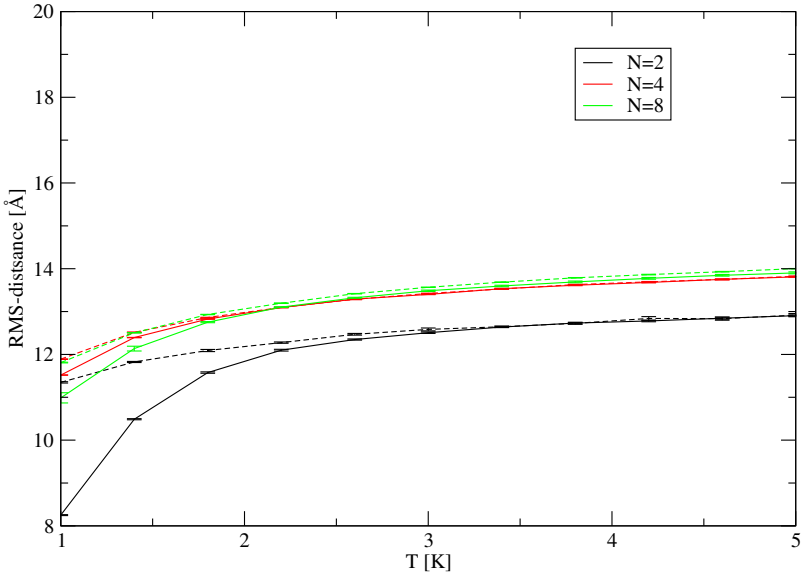

Figure 5.9. The average RMS-distance between interacting particles, of a variable amount, on a circular volume with diameter 30Å, and with 100 beads on the worldlines.

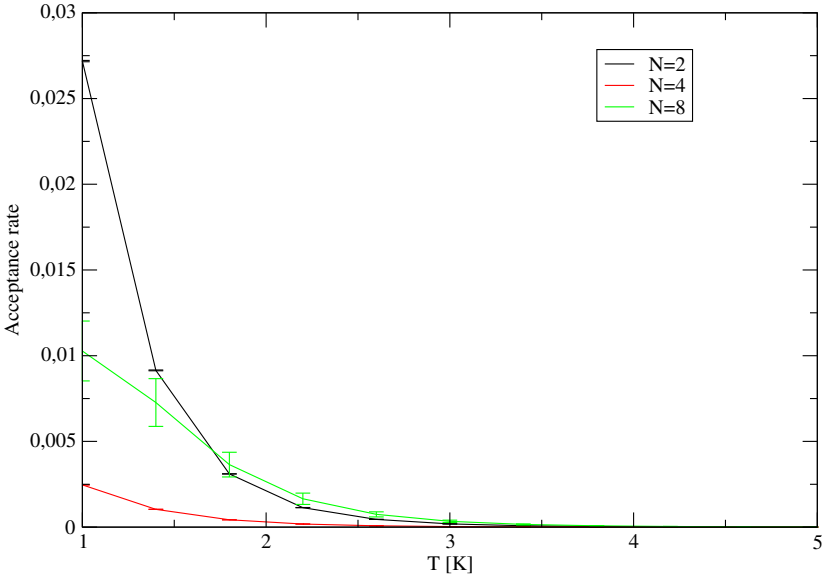

Figure 5.10. Success rate for the "swap-move" for bosonic systems with varying particle number on a circular volume with diameter 30Å and 100 beads on the worldlines.

It is also worth commenting the large error for $N = 8$, in particular in the heat capacity. We remind that we have used the a primitive approximation for the particle interaction (Eq. (3.12)). While the primitive approximation is exact for the case of $N = 2$, it has a slower rate of convergence for higher particle numbers, which is where higher order corrections become more relevant [3, 7].

The effect of the Bose-Einstein statistics occur at a much higher temperature than expected. Reasons for this is likely the lack of a periodic boundary in our simulation volume, which allows a smaller subset of the particles to effectively escape the potential wells of the other particles, and thus become free to entangle without interference from other helium atoms. The entangling done by the bosons should keep them trapped better in their respective potential wells, resulting in a smaller average RMS-distance. However, this effect is marginally seen at best. Neither system is close to the lattice constant for helium (3.570 Å). In both cases, the particles tend to escape their respective wells enough to diffuse all the way out to the wall. Had a periodic boundary been used, the particles would not have been able to escape their respective potential for small simulation volumes, and more entangling would likely have been observed in the bosonic system.

Chapter 6

Summary and Conclusions

In this thesis we have investigated the differences on low temperature ^{4}He models using boltzmannon and boson statistics. We have done this by implementing and utilizing a Metropolis-Hastings algorithm on a bounded 2D-space, looking at different parameter values for number of particles, beads on our worldlines, and sizes of our domains. To avoid cases of superfluidity and too long runtime, the temperature range investigated was kept above 1K.

We started with comparing how boltzmannons and bosons behave without any interaction between particles, and comparing it to the analytical solution of the problem. There were small differences in energy levels, as well as expected differences in the average RMS-distance between particles. A larger difference than expected was seen in the heat capacity, and seemed to depend heavily on the number of beads on the particle worldlines. A possible explanation to the differences could be due to finite-size errors.

We proceeded to compare the particles while they interacted with each other on the domain. We modeled the ^{4}He particles interaction by the semi-empirical Aziz potential, and used a primitive approximation that two particles interacted independently from other particles in the domain. We ran comparative simulations between boltzmannons and bosons for 2, 4, and 8 particles in the domain. The simulations showed an expected similar behaviour above 3K. Below this temperature, energy levels dropped and heat capacity quickly rose for the bosons, as the worldlines started to get entangled.

The resulting data showed a larger error with more particles in the domain, likely due to the primitive approximation not converging fast enough. Since the runtime for the 8 particle runs dated to a near month, it is not feasible to scale up the runtime to diminish the error without further optimizing the algorithm. A good start of such work would be to implement a higher-order correction of the interaction,

such as in Ref [7].

A future project could expand on the code to investigate superfluidity by adding periodic boundary conditions to the domain, add a third dimension - which would require very little work, but a great increase in simulation runtime. Once periodic boundaries in the spatial dimension, a third spacial dimension, and higher-order corrections are in place, the algorithm should be able to investigate the region near 0.1K. While simulations have been done with 64 particles in such a domain, the amount of computational resources needed would be staggering. It is possible to gain good data by using as little as four particles in this case [7]. It becomes of interest to track the *winding number* of the superfluid state in this region, and a subroutine that keeps track of this should be implemented as well. Furthermore, it would be of interest to investigate the effects of the worldline entanglements on the entropy, explained for example in the work by Herdman et al. [17].

Appendix A

Solution to the Schrödinger equation on a circle

We aim to solve the Schrödinger equation for a single particle in two dimensional circular domain

$$-\frac{\hbar^2}{2m}\left(\frac{\partial^2\psi}{\partial x^2}+\frac{\partial^2\psi}{\partial y^2}\right)+V(x,y)\psi(x,y)=E\psi(x,y) \tag{A.1}$$

$$V(x,y)=\begin{cases}0 & \text{if } r=\sqrt{x^2+y^2}<r_0\\ \infty & \text{if } r=\sqrt{x^2+y^2}>r_0\end{cases} \tag{A.2}$$

with the boundary conditions

$$\psi(r,\theta)=0 \text{ if } r>r_0 \tag{A.3}$$

$$\psi(r,\theta)\in\mathcal{C}^2\forall\ r,\theta. \tag{A.4}$$

We start by changing to polar coordinates $(x,y)\rightarrow(r,\theta)=\left(\sqrt{x^2+y^2},\arctan\left(\frac{y}{x}\right)\right)$. The Schrödinger equation becomes

$$-\frac{\hbar^2}{2m}\left(\frac{\partial^2}{\partial r^2}+\frac{1}{r}\frac{\partial}{\partial r}+\frac{1}{r^2}\frac{\partial^2}{\partial\theta^2}+V(r)\right)\psi(r,\theta)=E\psi(r,\theta). \tag{A.5}$$

Since the potential is zero inside the domain, the expression is reduced to Helmholtz equation

$$\left(\frac{\partial^2}{\partial r^2}+\frac{1}{r}\frac{\partial}{\partial r}+\frac{1}{r^2}\frac{\partial^2}{\partial\theta^2}\right)\psi(r,\theta)=-\underbrace{\frac{2mE}{\hbar^2}}_{=\epsilon}\psi(r,\theta). \tag{A.6}$$

We solve this equation by separation of variables

$$\psi(r,\theta) = R(r)\Theta(\theta), \tag{A.7}$$

which leads to the θ dependence being on the form

$$\Theta(\theta) = C \cdot e^{-in\theta}. \tag{A.8}$$

We solve for the r dependence

$$\left(\frac{\partial^2}{\partial r^2} + \frac{1}{r}\frac{\partial}{\partial r} + \left(\epsilon - \frac{n^2}{r^2}\right)\right) R(r) = 0. \tag{A.9}$$

We do a change of variable $\rho = kr$, where $k = \sqrt{1/\epsilon}$

$$\left(\rho^2\frac{\partial^2}{\partial \rho^2} + \rho\frac{\partial}{\partial \rho} + (\rho^2 - n^2\right) R(\rho) = 0. \tag{A.10}$$

If $\rho > 0$, the general solution is given by

$$R(r) = aJ_n(\rho) + bY_n(\rho), \tag{A.11}$$

where $J_n(\rho)$ and $Y_n(\rho)$ are the Bessel functions of first and second kind. For the function to be limited on the whole domain, we require $b = 0$. To achieve $\psi(r_0, \theta) = 0$ we require that

$$J_n\left(\frac{r_0}{\sqrt{\epsilon}}\right) = 0, \tag{A.12}$$

That is, the energy levels are given by

$$E_{n\nu} = \frac{\hbar^2}{2m}\left(\frac{\rho_{n\nu}}{r_0}\right)^2, \tag{A.13}$$

where $\rho_{n\nu}$ is the ν:th zero to the n:th Bessel function. Since the zeros are increasing $\rho_{n\nu} \leq \rho_{n\nu+1}$, the ground state is given as

$$E_{00} = \frac{\hbar^2}{2m}\left(\frac{\rho_{00}}{r_0}\right)^2 = \frac{\hbar^2}{2m}\left(\frac{2.4048}{r_0}\right)^2. \tag{A.14}$$

The average energy for the system is given as a usual by

$$E = \langle H \rangle = \frac{\sum_{n,\nu} E_{n\nu} e^{-\beta E_{n\nu}}}{\sum_{n,\nu} e^{-\beta E_{n\nu}}}. \tag{A.15}$$

Since there are infinitely many zeros of the Bessel function, we can rewrite the last expression as an integral

$$\langle H \rangle = \frac{1}{\beta}\frac{\int_{\sqrt{\beta E_{00}}}^{\infty} \mathrm{d}x x^2 e^{-x^2}}{\int_{\sqrt{\beta E_{00}}}^{\infty} \mathrm{d}x e^{-x^2}} = k_B T\left(\frac{1}{2} + \frac{\sqrt{\beta E_{00}} e^{-\beta E_{00}}}{\sqrt{\pi}\,\mathrm{erf}\left(\sqrt{\beta E_{00}}\right)}\right). \tag{A.16}$$

The limits of interest are

$$\lim_{E_{00}\to 0} k_B T \left(\frac{1}{2} + \frac{\sqrt{\beta E_{00}} e^{-\beta E_{00}}}{\sqrt{\pi}\,\mathrm{erf}\left(\sqrt{\beta E_{00}}\right)} \right) = k_B T, \tag{A.17}$$

$$\lim_{E_{00}\to \infty} k_B T \left(\frac{1}{2} + \frac{\sqrt{\beta E_{00}} e^{-\beta E_{00}}}{\sqrt{\pi}\,\mathrm{erf}\left(\sqrt{\beta E_{00}}\right)} \right) = \frac{1}{2} k_B T. \tag{A.18}$$

For n non-interacting particles the energy becomes

$$E(n) = nE. \tag{A.19}$$

Bibliography

[1] P. Kapitza, *Viscosity of Liquid Helium below the λ-Point*, Nature **141**, 74 (1938).

[2] J. F. Allen and A. D. Misener, *Flow Phenomena in Liquid Helium II*, Nature **142**, 643 (1938).

[3] L. Barberà and J. Medico, *Path integral Monte Carlo: algorithms and applications to quantum fluids* (Universitat Politècnica de Catalunya, 2002).

[4] R. P. Feynman, *Space-Time Approach to Non-Relativistic Quantum Mechanics*, Rev. Mod. Phys. **20**, 367 (1948).

[5] W. Heisenberg, Über quantentheoretische umdeutung kinematischer und mechanischer beziehungen, Original Scientific Papers Wissenschaftliche Originalarbeiten, pp. 382–396, Springer, 1985.

[6] E. Schrödinger, *An Undulatory Theory of the Mechanics of Atoms and Molecules*, Phys. Rev. **28**, 1049 (1926).

[7] D. M. Ceperley, *Path integrals in the theory of condensed helium*, Rev. Mod. Phys. **67**, 279 (1995).

[8] N. Metropolis *et al.*, *Equation of State Calculations by Fast Computing Machines*, The Journal of Chemical Physics **21**, 1087 (1953).

[9] E. Newman and G. Barkema, *Monte Carlo Methods in Statistical Physics* (Clarendon Press, 1999).

[10] M. Matsumoto and T. Nishimura, *Mersenne Twister: A 623-dimensionally Equidistributed Uniform Pseudo-random Number Generator*, ACM Trans. Model. Comput. Simul. **8**, 3 (1998).

[11] H. F. Trotter, *On the Product of Semi-Groups of Operators*, Proceedings of the American Mathematical Society **10**, pp. 545 (1959).

[12] K. Mainz, *Monte Carlo and Molecular Dynamics Simulations in Polymer Science* (Oxford University Press, USA, 1995).

[13] R. A. Aziz *et al.*, *An accurate intermolecular potential for helium*, The Journal of Chemical Physics **70**, 4330 (1979).

[14] D. M. Ceperley and E. Pollock, *Path-Integral Computation Techniques for Superfluid ^4He*, In Caracciolo, S. and Fabrocini, A., editors, *Monte Carlo methods in theoretical physics* , 35 (1992).

[15] M. Sprik, M. L. Klein and D. Chandler, *Staging: A sampling technique for the Monte Carlo evaluation of path integrals*, Phys. Rev. B **31**, 4234 (1985).

[16] M. Boninsegni, *Permutation Sampling in Path Integral Monte Carlo*, Journal of Low Temperature Physics **141**, 27 (2005).

[17] C. M. Herdman *et al.*, *Path-integral Monte Carlo method for Rényi entanglement entropies*, Phys. Rev. E **90**, 013308 (2014).